ACADÉMIE
DES SCIENCES
INSTITUT DE FRANCE

Comptes Rendus
Mécanique

Rachele Allena, Daria Scerrato, Alberto Bersani and Ivan Giorgio

Simulating bone healing with bio-resorbable scaffolds in a three-dimensional system: insights into graft resorption and integration

Volume 353 (2025), p. 479-497

Online since: 10 March 2025

https://doi.org/10.5802/crmeca.291

The Comptes Rendus. Mécanique *are a member of the Mersenne Center for open scientific publishing*
www.centre-mersenne.org — e-ISSN : 1873-7234

ACADÉMIE DES SCIENCES
INSTITUT DE FRANCE

Comptes Rendus. Mécanique
2025, Vol. 353, p. 479-497
https://doi.org/10.5802/crmeca.291

Research article / *Article de recherche*

Simulating bone healing with bio-resorbable scaffolds in a three-dimensional system: insights into graft resorption and integration

Simulation de la cicatrisation osseuse avec des échafaudages bio-résorbables dans un système tridimensionnel : aperçus sur la résorption et l'intégration des greffes

Rachele Allena[a,*,b], **Daria Scerrato**[c,d], **Alberto Bersani**[c,d,e] and **Ivan Giorgio**[f,d,e]

[a] Université Côte d'Azur, Laboratoire Jean Alexandre Dieudonné UMR CNRS 7351, Nice, France

[b] Institut Universitaire de France, France

[c] Dipartimento di Ingegneria Meccanica e Aerospaziale (DIMA), University of Rome La Sapienza, Italy

[d] International Research Center for the Mathematics and Mechanics of Complex Systems (M&MoCS), University of L'Aquila, Italy

[e] Gruppo Nazionale per la Fisica Matematica (GNFM) of the Istituto Nazionale di Alta Matematica (INdAM, Italy), Italy

[f] Dipartimento di Ingegneria Civile, Edile-Architettura e Ambientale (DICEAA), University of L'Aquila, Italy

E-mail: rachele.allena@univ-cotedazur.fr (R. Allena)

Abstract. This study introduces a three-dimensional (3D) model for investigating the interactions between trabecular bone tissue and bio-resorbable grafts, focusing on their role in bone remodelling processes. Using principles of poroelasticity, the model captures the mechanical behaviour of both bone and graft as porous continua, with their interaction influenced by time-varying mechanical loads and diffusive mechanical stimuli. The stimuli, originating from the strain energy density, propagate through the system, triggering bone formation and graft resorption across distant regions. Numerical simulations reveal the critical impact of load frequency and intensity on remodelling efficiency, with higher values promoting improved bone density and graft integration. This 3D approach provides information on optimizing scaffold design, offering valuable guidance to improve clinical outcomes in bone repair and regeneration procedures.

Résumé. Cette étude présente un modèle tridimensionnel (3D) destiné à explorer les interactions entre le tissu osseux trabéculaire et les greffes bio-résorbables, en se concentrant sur leur rôle dans les processus de remodelage osseux. En s'appuyant sur les principes de la poroélasticité, le modèle reproduit le comportement mécanique de l'os et de la greffe en tant que milieux poreux, dont l'interaction est influencée par des charges mécaniques variables dans le temps et par des stimuli mécaniques diffusifs. Ces stimuli, issus de

* Corresponding author

la densité d'énergie de déformation, se propagent à travers le système, déclenchant la formation osseuse et la résorption des greffes dans des régions éloignées. Les simulations numériques mettent en évidence l'impact déterminant de la fréquence et de l'intensité des charges sur l'efficacité du remodelage, des valeurs plus élevées favorisant une densité osseuse accrue et une meilleure intégration des greffes. Cette approche 3D fournit des informations précieuses pour optimiser la conception des échafaudages, offrant ainsi des recommandations utiles pour améliorer les résultats cliniques en matière de réparation et de régénération osseuse.

Keywords. Bone remodelling, Bone–graft interaction, Porous resorbable scaffold, Fick's laws of diffusion, Biomechanical stimulus.

Mots-clés. Remodelage osseux, Interaction os–greffe, Échafaudage poreux résorbable, Lois de diffusion de Fick, Stimulus biomécanique.

Manuscript received 9 December 2024, revised 11 February 2025, accepted 18 February 2025.

1. Introduction

Bone remodelling is a lifelong process that maintains bone strength and functionality by replacing old or damaged bone with new tissue, ensuring structural integrity of the skeleton. This process is driven by the orchestrated activities of osteoclasts, which resorb bone, and osteoblasts, which form new bone. At the core of this process are osteocytes, which act as mechanosensors, detecting mechanical stimuli and coordinating the actions of osteoclasts and osteoblasts. The stimuli sensed by osteocytes originate from the mechanical loads applied to bones during daily activities, such as walking or exercising. Bone tissue responds by adapting its architecture and density to meet the mechanical demands placed upon it, a phenomenon known as mechanotransduction [1,2].

Mechanotransduction involves converting mechanical signals into biochemical responses, triggering bone remodelling processes that either strengthen the bone by increasing its density or weaken it by resorbing less-needed areas. Dynamic loads, particularly those from physical activity, are essential to stimulate bone remodelling. These loads induce mechanical strains within the bone that are perceived by osteocytes. In regions subjected to high mechanical strain, osteoblasts are activated to synthesize new bone, leading to localized bone formation. Conversely, osteoclasts are activated to resorb bone in regions of low mechanical strain, resulting in bone loss [1]. Thus, bone architecture and mass distribution are optimized to withstand mechanical forces, preventing fracture or deformation [2,3].

The process of bone remodelling is influenced not only by mechanical forces but also by biochemical and cellular factors. Calcium homeostasis and repair of micro-damages from daily stresses are other critical functions of bone remodelling [1,4]. Furthermore, the complexity of this process is reflected in the interactions between cells and their surrounding environment (see, e.g., [5] for a similar mechanism of functioning). Various signalling pathways are involved, particularly the diffusion of mechanical stimuli within the bone matrix. These stimuli guide osteocytes in assessing the mechanical environment and regulating bone adaptation accordingly [6,7].

The role of mechanical stimuli in bone remodelling has been the focus of numerous theoretical and experimental studies. Traditional models of bone remodelling often treated the mechanical stimulus as localized, affecting only the region where the strain occurred [8,9]. However, recent advances suggest that a diffusive model better reflects the behaviour of actual bone tissue [10]. By considering the stimulus as a diffusive agent, some models account for the influence of mechanical loads on a larger area, improving the accuracy of predictions regarding bone adaptation. The stimulus is assumed to propagate through the bone matrix, influenced by the microstructure of the tissue, such as its porosity. This propagation affects osteocyte activity and,

consequently, bone resorption and formation rates [11]. These models consider the stimulus as a function of the strain energy density generated by mechanical loads. In this context, the strain energy density serves as the source of the stimulus, which diffuses through the bone tissue, initiating the remodelling response in distant regions. The diffusive nature of the stimulus allows it to propagate throughout the tissue, allowing a coordinated cellular response throughout the bone structure, even in areas that do not experience direct mechanical loads [7,8].

In addition to biological factors, the structural characteristics of bone tissue, such as porosity, play a significant role in bone remodelling. Bone is a composite material composed of a solid phase consisting of collagen and mineral components, and a porous phase filled with fluids such as blood and bone marrow. The porous nature of bone allows the diffusion of nutrients and signalling molecules, which are essential for cell migration and function. Porosity also affects the mechanical properties of bone, influencing how mechanical loads are distributed within tissue [12,13].

The remodelling process is crucial not only for maintaining bone health but also for healing bone injuries and defects. In clinical settings, the use of bio-resorbable scaffolds to repair bone defects has become an area of significant interest. These scaffolds are designed to integrate with bone tissue and support mechanical loads during healing. For effective bone healing, the scaffold must have suitable mechanical properties, such as stiffness and toughness, and must also be porous enough to allow cell migration and diffusion of signalling molecules [7,14]. The porosity of the scaffold is particularly important because it facilitates the invasion of osteogenic cells and the formation of new bone while at the same time providing structural support until the scaffold is resorbed and replaced by natural bone tissue [15]. The porosity concurs to define the microstructure of bone tissue and can also be replicated in the graft to facilitate osteointegration [16], but to have a complete picture of the mechanical behaviour of a system treated with a bio-resorbable scaffold, it could be necessary, under some conditions, to generalize the mechanical description in the sense of [17], with generalized models that include micropolar effects, grain interactions, inclusions, fibres, etc. [18–25]. Biological systems, such as our system, composed of bone tissue, an implant, cellular networks, and equipped by physiological processes, exhibit highly complex and interconnected dynamics. These systems are often influenced by a multitude of factors, including genetic, environmental, and stochastic variations, which introduce inherent uncertainties. Accurate modelling of such systems requires accounting for these uncertainties, as they can significantly impact system behaviour and predictions. By incorporating probabilistic approaches and sensitivity analyses, it is possible to capture the variability and unpredictability that are fundamental to understanding and effectively simulating biological complexity (see, e.g., [26–28] regarding the role of uncertainties in multiscale mechanics).

Mathematical models have been developed to study the interaction between bone tissue and bio-resorbable scaffolds. These models aim to optimize the design of scaffolds by predicting how their mechanical and geometric properties influence the bone healing process [29,30]. For instance, a recent study employed a diffusive model to analyze the interactions between bone and a resorbable graft, focusing on how mechanical stimuli influence the rates of bone formation and graft resorption [31,32]. The results of this study highlighted the importance of scaffold porosity and mechanical properties in promoting effective bone regeneration. By simulating different scaffold designs, such models provide valuable insight that can guide the development of more efficient bone repair strategies.

The present study represents a significant extension of our previous work by introducing a three-dimensional (3D) system that includes both bone and bio-resorbable grafts, enhancing the realism of the model in simulating the bone remodelling process. The new model simulates the interaction between bone tissue and the graft, considering how mechanical loads affect both components over time. As in [12], we use a diffusive signal to represent the mechanical stimulus,

which originates from the strain energy density generated by dynamic loads and propagates through both the bone and the graft. Additionally, our model is developed within a poroelastic framework. As such, it implicitly takes into account the interplay between interstitial fluid flow and solid deformation. This constitutes an important feature, as osteocytes are known to be sensitive to fluid-induced shear stress. The pressure gradients that result inside the porous bone matrix contribute to fluid flow, which can cause shear stress on osteocytes and their dendritic processes. Although our model does not explicitly resolve the flow of the microscale canalicular network, it captures a global description of bone remodelling, combining indirect fluid-driven stimuli and direct solid-phase strains into a single mathematical framework. We account for these effects through the poroelastic formulation, which inherently couples the solid and fluid phases of bone and graft materials. The poroelastic framework considers the influence of interstitial fluid by incorporating: (1) strain rate effects, where viscosity effects interact with the deforming solid skeleton, influencing local mechanical stimuli; (2) pressure-dependent deformations, allowing for an indirect representation of fluid-induced mechanical signals; (3) pore evolution, which modifies the permeability and mechanical response of the system over time. This approach allows us to evaluate how changes in porosity and loading conditions influence both the spatial and temporal evolution of mechanical signals in the system.

Previous models for bone remodelling have evolved to incorporate mechanical stimuli, poroelastic effects, and scaffold bioresorption, progressively improving their ability to simulate real physiological conditions. This study builds on two key prior works: one that introduced a 2D bone/graft model with a diffusive stimulus approach for bone remodelling but did not extend to full 3D effects or dynamic loading [7], and another one that analyzed the influence of loading frequency on bone remodelling within a 3D bone structure, but without incorporating a bioresorbable scaffold [12]. Although these studies provided valuable information, they did not address the combined effects of cyclic mechanical loading and scaffold integration in a 3D bone/graft system, which is the focus of the present work.

Indeed, a key novelty of this study lies in the first integration of a three-dimensional bioresorbable scaffold (BGB) within a trabecular bone matrix under dynamic loading conditions. Unlike previous models that were either limited to two dimensions or considered only the bone response without scaffold interaction, this approach allows for a more comprehensive and physiologically relevant simulation of scaffold remodelling dynamics. The study also extends classical bone remodelling models by incorporating poroelasticity, which enables the interaction between solid deformation and interstitial fluid flow—an essential factor in osteocyte mechanotransduction. This approach enables a more realistic representation of how oscillatory mechanical forces influence both bone remodelling and graft resorption over time, providing deeper insight into the role of mechanical stimulation in optimizing scaffold integration and bone regeneration. This work also investigates how dynamic mechanical loads distribute stress and strain within the bone/graft system, rather than relying on static or simplified loading conditions as in previous studies. By integrating a 3D scaffold, dynamic mechanical loading, poroelastic effects, and diffusive remodelling stimuli, this study aims to represent a significant step forward in computational modelling of bone healing. The results offer critical information for optimizing both scaffold design and rehabilitation protocols, contributing to advancements in orthopedic applications and tissue engineering strategies. By incorporating both bone and graft materials into the model, this study can provide valuable information about how graft mechanical properties and porosity influence the bone healing process. The diffusion of the mechanical stimulus is crucial, as it enables the signal to reach regions far from the immediate site of the load, promoting a coordinated response between bone formation and graft resorption. This is particularly relevant in clinical contexts where bio-resorbable scaffolds are used to support bone healing after injury or surgery.

The findings of this study improve our understanding of bone/graft interactions, highlighting the role of mechanical stimuli in driving the remodelling process in both bone and graft materials. By simulating a 3D system, the model can capture the complex interaction between these materials under dynamic mechanical loads, providing a powerful tool to optimize scaffold design and improve clinical outcomes in bone repair procedures [8,11,33].

2. The model

Similarly to our previous works [7,34], let us consider a 3D system composed of trabecular bone tissue implanted with a bio-resorbable scaffold. Both bone and graft materials exhibit porosity: lacunar-canalicular, inter-trabecular, or collagen-apatites porosity for the bone and interconnected inner cavities for the graft. Consequently, we treat them as porous continua and their mechanical behaviour is governed by the principles of poroelasticity [11] and [35–39].

The kinematical descriptors that characterize our model are the displacement $\mathbf{u}$ and the current Lagrangian porosity ϕ, which are defined as follows:

$$\mathbf{u} = \mathbf{x} - \mathbf{X}$$
$$\phi(\mathbf{X}, t) = n[\chi(\mathbf{X}, t)]J(\mathbf{X}, t)$$

where $\mathbf{X}$ is any particle of the system in the reference configuration, $\mathbf{x} = \chi(\mathbf{X}, t)$ is the position of the particle $\mathbf{X}$ in the current configuration, $n[\chi(\mathbf{X}, t)]$ is the Eulerian porosity and $J = \det(\mathbf{F}) = \det(\nabla\chi(\mathbf{X}, t))$ [40].

Throughout evolution, the stiffness of the bone/graft system may attain significantly softer values than the initial measurements, resulting in a deformed structure that differs from the reference state. To ensure consistency, we incorporate nonlinear behaviour most straightforwardly while assuming that the system remains within the elastic response range. Furthermore, the rationale for this choice is attributed to the intricacy of bone microstructure, specifically the trabeculae, which can exhibit non-linear behaviours even within a minor strain regime, as evidenced in [41].

The adopted poroelastic model describes the interaction between a porous elastic solid and an interstitial fluid. It accounts for fluid flow through the porous structure and the resulting mechanical deformations. In the context of bone remodelling, this formulation allows us to take into account permeability effects; the model naturally incorporates porosity and permeability, which influence fluid flow in the lacunar-canalicular network. Increased porosity typically improves permeability, leading to changes in interstitial fluid flow and the shear stress sensed by osteocytes. Furthermore, such a model captures how external mechanical loads induce pressure gradients that drive fluid through the network, generating mechanical stimuli critical for osteocyte signaling and bone remodelling.

The mechanical response of the system is described by the finite-strain tensor $\mathbf{E}_{ij}(\mathbf{X}, t)$

$$\mathbf{E}_{ij}(\mathbf{X}, t) = \tfrac{1}{2}(u_{i,j} + u_{j,i} + u_{i,k}u_{k,j})$$

and the deformation measure for porosity $\zeta(\mathbf{X}, t)$ [42] reads

$$\zeta(\mathbf{X}, t) = \phi(\mathbf{X}, t) - \phi^*(\mathbf{X}, t)$$

with $\phi(\mathbf{X}, t)$ and $\phi^*(\mathbf{X}, t)$ the Lagrangian porosities in the current and reference configurations, respectively. Therefore, ζ can be associated with the change in the fluid content between the reference to the current configuration.

Although the system consists of two components—the bioresorbable graft and the bone—it can be examined as a whole using mixture theory. To be more precise, the bone exhibits a solid phase as well as a porous region that is usually occupied by interstitial fluids, blood,

bone cells, and bone marrow. The graft exhibits porosity as well; upon implantation, its pores are immediately filled with living things [15,43,44]. Despite having relatively identical starting conditions, the two portions grow differently over time. In actuality, three phases can coexist in the graft during the remodelling process: bioresorbable material, bone, and physiological fluid.

Accordingly, $\phi^*(\mathbf{X}, t)$ can be written as

$$\phi^*(\mathbf{X}, t) = 1 - \left(\frac{\rho_{\mathrm{b}}^*(\mathbf{X}, t)}{\hat{\rho}_{\mathrm{b}}} + \frac{\rho_{\mathrm{g}}^*(\mathbf{X}, t)}{\hat{\rho}_{\mathrm{g}}} \right) \tag{1}$$

where $\rho_{\mathrm{b}}^*(\mathbf{X}, t)/\hat{\rho}_{\mathrm{b}}$ and $\rho_{\mathrm{g}}^*(\mathbf{X}, t)/\hat{\rho}_{\mathrm{g}}$ are the volume fractions of the constituents and ρ_{b}^* and ρ_{g}^* are the apparent mass densities of bone tissue and graft artificial material in the reference configuration, respectively. The superimposed hat indicates the mass densities evaluated considering the precise volume occupied by those phases. Since the apparent mass densities of different phases depend on environment mechanical excitations and time, we assume that the reference configuration is linked to the apparent mass density in the reference state, i.e., when zero stress occurs. We assume that the reference configuration is related to the apparent mass density in the reference state, or when zero stress occurs, since the apparent mass densities of different phases rely on time and mechanical excitations in the environment. In consideration of the aforementioned definitions, the current porosity ϕ can be expressed as

$$\phi = \phi^* + \zeta. \tag{2}$$

The total energy density of the system is given by [45,46]

$$\begin{aligned} \mathscr{E} = U_s + U_f + U_{fs} = {} & \underbrace{\tfrac{1}{2}\lambda(\rho_{\mathrm{b}}^*, \rho_{\mathrm{g}}^*)E_{ii}E_{jj} + \mu(\rho_{\mathrm{b}}^*, \rho_{\mathrm{g}}^*)E_{ij}E_{jj}}_{U_s} \\ & + \underbrace{\tfrac{1}{2}K_1(\rho_{\mathrm{b}}^*, \rho_{\mathrm{g}}^*)\zeta^2}_{U_f} + \underbrace{\tfrac{1}{2}K_2(\rho_{\mathrm{b}}^*, \rho_{\mathrm{g}}^*)\zeta E_{ii}}_{U_{fs}} \end{aligned} \tag{3}$$

where all material parameters are considered as a function of the apparent mass density of the bone and the graft evaluated in the reference configuration. The subscripts represent the solid part (s), the fluid part (f), and the fluid–solid coupling (fs) in the given order. Such an expression is the simplest when considering bone and graft as isotropic materials (see, e.g., [47] for generalization).

λ and μ are the Lamé coefficients and read

$$\lambda = \frac{\nu Y(\rho_{\mathrm{b}}^*, \rho_{\mathrm{g}}^*)}{(1+\nu)(1-2\nu)}, \quad \mu = \frac{Y(\rho_{\mathrm{b}}^*, \rho_{\mathrm{g}}^*)}{2(1+\nu)} \tag{4}$$

with the overall Young modulus:

$$Y = Y_{\mathrm{b}}^{\max}\left(\frac{\rho_{\mathrm{b}}^*}{\hat{\rho}_{\mathrm{b}}}\right)^2 + Y_{\mathrm{g}}^{\max}\left(\frac{\rho_{\mathrm{g}}^*}{\hat{\rho}_{\mathrm{g}}}\right)^2 \tag{5}$$

where $Y_{\mathrm{b}}^{\max}$ and $Y_{\mathrm{g}}^{\max}$ are the maximal values of the Young moduli for the bone and the graft, respectively. For simplicity, the Poisson ratio can be assumed to be constant and given. Conversely, we should consider two evolution rules for the Young moduli and the Poisson ratios, as discussed in [48,49] or, in a broader context, in [50]. This approach enhances accuracy, but also increases complexity and, in many contexts, this level of detail is not even necessary. K_1 is a compressibility coefficient defined as the volume of fluid released from unit bulk volume per unit decrease in pore pressure under the condition of constant confining stresses [34,45]. K_2 couples the micro-structure due to pores and the bulk solid [34,45]. The expressions of K_1 and K_2 can be found in [34]. As mentioned in [7,34], the fluid that fills the pores, the solid matrix of the bone, the contact between the solid and fluid phases, and the interface between the graft and the bone

are some possible locations for dissipation in the system. All these sources are taken into account via a Rayleigh functional as follows:

$$2\mathscr{D}_s = 2\mu^v(\dot{E}_{ij}\dot{E}_{ij} - \tfrac{1}{3}\dot{E}_{ii}\dot{E}_{jj}) + k^v\dot{E}_{ii}\dot{E}_{jj} \tag{6}$$

employing a Kelvin–Voigt model, where $\dot{E}$ is the solid–fluid rate of deformation and μ^v and k^v are two viscous coefficients.

Bone remodelling occurs over multiple time scales. Two-time scales are commonly involved in the overall process. The first is a fast-varying time scale associated with mechanical loading cycles, such as those generated by walking or exercising. These loads typically oscillate with frequencies in the range of seconds to minutes [51] and induce instantaneous mechanical responses in the bone/graft system. The second is a slow-varying time scale that governs the long-term adaptation of bone density and porosity due to mechanotransduction processes, which evolve over weeks to months [52]. In this paper, we adopt an approach that follows a well-separated time scale assumption, where rapid oscillations of the mechanical load contribute to the mechanical stimulus indirectly affecting the evolution of the long-term parameters of the material. This allows us to analyze bone remodelling dynamics without resolving each individual loading cycle, consistent with previous studies that employ similar temporal separation strategies in mechanobiological modelling. Therefore, only the slow-varying-time scale is considered, as the rapid oscillations due to the former fast-varying-time scale can be treated from the perspective of well-separated time scales, as explained in [31].

The Generalized Principle of Virtual Work is as follows:

$$\int_{\mathscr{B}^*}\delta\mathscr{E}\,\mathrm{d}\mathscr{B}^* + \int_{\mathscr{B}^*}\frac{\partial\mathscr{D}_s}{\partial\dot{E}_{ij}}\delta E_{ij}\partial\mathscr{B}^* = \int_{\mathscr{B}^*}\delta\mathscr{W}^{\mathrm{ext}}\,\mathrm{d}\mathscr{B}^* \tag{7}$$

where $\delta\mathscr{W}^{\mathrm{ext}}$ is the virtual work generated by the external loads, which can be written as

$$\delta\mathscr{W}^{\mathrm{ext}} = \int_{\partial_\tau\mathscr{B}^*}\tau_i\delta u_i\,\mathrm{d}\mathscr{S}^* + \int_{\partial_\Xi\mathscr{B}^*}\Xi\delta\zeta\,\mathrm{d}\mathscr{S}^*. \tag{8}$$

In this equation the first term indicates the forces per unit surface (i.e., τ_i on the part of the boundary $\delta_\tau\mathscr{B}^*$) and the second term relates to the effects of a pore pressure Ξ on the boundary $\delta_\Xi\mathscr{B}^*$. In this study, since we focus solely on the slow-varying time scale, we can neglect the effects of inertia. To fully understand these effects (as shown in similar complex structures, see, e.g., [53,54]), it would be necessary to introduce a fast-varying time scale. However, as previously remarked, for the sake of simplicity, we have chosen not to include that in this work.

Once the graft has been implanted, bone remodelling takes place around it and, after a while, also within it. We describe the evolution over time of the apparent mass density of the bone (ρ_{b}) and the graft (ρ_{g}) with respect to the reference configuration as follows:

$$\begin{cases}\dfrac{\partial\rho_{\mathrm{b}}^*}{\partial t}(\mathbf{X},t) = A_{\mathrm{b}}[S(\mathbf{X},t)]\,H[\phi(\mathbf{X},t)] \quad \text{with } 0<\rho_{\mathrm{b}}^*\le\hat{\rho}_{\mathrm{b}}\\[2ex] \dfrac{\partial\rho_{\mathrm{g}}^*}{\partial t}(\mathbf{X},t) = A_{\mathrm{g}}[S(\mathbf{X},t)]\,H[\phi(\mathbf{X},t)] \quad \text{with } 0<\rho_{\mathrm{g}}^*\le\rho_{\mathrm{g}}^*(\mathbf{X},0)\end{cases} \tag{9}$$

where $S(\mathbf{X},t)$ is the mechanical stimulus and A_{b} and A_{g} are two functions assumed to be piecewise linear as follows:

$$A_{\{\mathrm{b,g}\}}[S(\mathbf{X},t)] = \begin{cases} s_{\{\mathrm{b,g}\}}[S(\mathbf{X},t) - S_s] & \text{for } (S-S_s)\ge 0\\ 0 & \text{for } S_r > S > S_s\\ r_{\{\mathrm{b,g}\}}[S(\mathbf{X},t) - S_r] & \text{for } (S-S_r)\le 0.\end{cases} \tag{10}$$

The notation $\cdot_{\{b,g\}}$ has been introduced to combine two formulas into a single, unified expression. The coefficients s and r represent the rates of growth and resorption, respectively, with the subscripts b, g denoting bone and graft, respectively. The quantities S_s and S_r serve as two thresholds that define the "lazy zone", which corresponds to the homeostatic state. These reference values of the stimulus are assessed with the understanding that they are energy-based. Consequently, we establish an assumed typical range of strain between 600 and 2000 microstrains from which we subsequently calculate the corresponding energy associated with that level of deformation. It has to be noticed that $s_g = 0$. In fact, we assume that the scaffold material degrades over time without undergoing new formation, whereas bone can grow in response to mechanical stimuli ($s_b > 0$). This assumption is consistent with the behavior of most bioresorbable materials, which are designed to be gradually resorbed and replaced by new bone tissue rather than self-renewing. Additionally, we have set $r_g = r_b$. We are aware that kinetics of bone resorption and scaffold degradation are governed by distinct biological and physicochemical processes. Bone resorption is primarily regulated by osteoclast activity, whereas scaffold resorption depends on several factors (i.e. hydrolysis, enzymatic degradation...). Nonetheless, this assumption ensures that resorption occurs at comparable rates in both materials, facilitating a direct comparison of their evolution under mechanical stimulation. In addition, it is a good practice that when designing the graft, the properties of the inserted material closely align with those of the original bone tissue. This adherence is crucial to ensure the optimal functionality of the replacement material. A significant disparity in the behavior of the graft compared to the native bone can lead to complications in both the short- and long-term reconstruction processes.

In this work, we adopt a classical approach grounded in phenomenological evolution rules. However, this simplification can be easily improved through variational methods, as outlined in [55,56].

During the remodelling process, porosity is crucial and is taken into account by the function $H[\phi(\mathbf{X}, t)]$. The pores facilitate the access of bone cells to the more remote regions of the system, allowing them to resorb or generate bone tissue in reaction to external forces. Thus, two potential results arise: (i) inadequate porosity hinders remodelling because no room is left for the bone cells to operate, or (ii) excessive porosity fails to support bone cells, both resulting in unchanging densities. Consequently, we have assumed that porosity reaches a maximum value of H at approximately 0.6, which provides optimal conditions for bone remodelling when porosity is distanced from the two extreme scenarios [10].

Traditionally, osteocytes perceive the mechanical stimulus $S(\mathbf{X}, t)$, allowing the bone to assess and modify its overall state.

Here, we assume that the solid phases—and, by extension, the mechanical properties—are altered by both osteoclasts and osteoblasts. As we have previously proposed in [7,10,12], the stimulus is defined via a diffusion equation.

$$\frac{\partial S}{\partial t} - \kappa \Delta S + \beta S = f(\rho_b^*)\mathscr{E} \tag{11}$$

with κ and β being two scalars; β is only activated when the stimulus is produced ($S > 0$), and it is associated with a metabolic resorption of the stimulus that prevents excessive accumulation of the stimulus. Here, we assume that κ and β are the same in scaffold and bone. Nonetheless, we are aware that the actual properties of these two materials may vary in terms of porosity and microstructure. This simplification allows us to focus on the basic phenomena of dynamic loading and mechanotransduction. The function $f(\rho_b^*)$ is a proper signalling weight as defined in [12] and reads

$$f(\rho^*) = \frac{1}{2}\left\{\tanh\left[20\left(\frac{\rho^*}{\hat{\rho}} - 0.15\right)\right] + \tanh[20(1-0.15)]\right\}. \tag{12}$$

This function depends on the apparent mass density of the tissue and increases monotonically. Assuming, as a first approximation, that osteocytes are distributed nearly equally throughout the tissue, we can infer that their density per unit volume is proportionate to the volume fraction.

The stimulus is equal to 0 and 367.57 J in the graft and in the bone, respectively, at the initial time $t = 0$. In the graft, the initial stimulus S is zero because at the beginning there are no osteocytes capable of producing it. In bone tissue, the initial stimulus is set within the range of the homestatic state ($S_r > S > S_s$); therefore, we start from an equilibrium state. Additionally, no stimulus is exchanged with the outside along the boundaries of the system.

In general, in the biological system considered, the accuracy of the models is heavily based on the precise estimation of parameters, which represent rates, thresholds, or interactions within the system. Given the inherent complexity and the potential lack of direct measurability, parametric evaluation through proper identification procedures becomes essential. These procedures, often involving optimization techniques, statistical inference, or other ad hoc methods, aim to reconcile models with experimental or observational data. By systematically refining parameter estimates, such methods improve model reliability and predictive power, allowing deeper insight into the underlying biological processes and better handling of uncertainties intrinsic to these systems [57–61]. In this study, we did not perform a formal parameter identification procedure. Instead, the model parameters were estimated through numerical calibration, ensuring that the simulated response captured key qualitative aspects observed in experimental studies. Our primary objective at this stage was to investigate the qualitative influence of mechanical loading on bone remodelling, rather than to achieve a precise quantitative fit with experimental data. This approach allowed us to explore fundamental trends, assess the sensitivity of the model to different mechanical stimuli, and identify relevant parameter ranges for future refinement. A more rigorous parameter identification process, which incorporates the fitting of experimental data and the quantification of uncertainties, is planned for subsequent studies to enhance the predictive accuracy of the model.

3. Numerical implementation for an illustrative case

In this work, the numerical investigations were carried out using the COMSOL Multiphysics software. A weak formulation that applies finite element analysis was used to directly solve the partial differential equations that constitute the previously described mathematical model. We employ this direct approach to create a sufficiently accurate model that utilizes the general-purpose capabilities of the chosen software, even if it may not be highly efficient. In the second stage of development, we can apply numerical procedures that are appropriately optimized for the model generated in the previous steps (see, e.g., [62,63]).

We consider a cylinder of length L and radius r, which represents a typical femoral diaphysis. The specimen is composed of bone at the bottom and at the top and by a graft of length L_g in the middle, resulting in a BGB structure (Figure 1). The cylinder is fully constrained at the bottom, while on the top surface, a sinusoidal force producing torsion and a pressure are applied as follows:

$$f = (X_2\mathbf{e_2} - X_1\mathbf{e_1})F_0 \sin(2\pi\Omega t) - [F_1 + F_2 \sin(2\pi\Omega t)]\mathbf{e_3} \tag{13}$$

where F_0, F_1 and F_1 are nominal forces, Ω is the frequency, and $\mathbf{e_1}, \mathbf{e_2}$ and $\mathbf{e_3}$ are the unit vectors of the coordinate system. We remark that Ω denotes a frequency that gradually changes over a period of weeks to months and does not capture the rapid frequency at the mechanical load time scale, consistent with the assumption of well-separated time scales. In fact, while the applied load in our model is oscillatory (at the slow-varying time scale), its influence on tissue adaptation is considered through the cumulative mechanical stimulus, which integrates the effects of strain

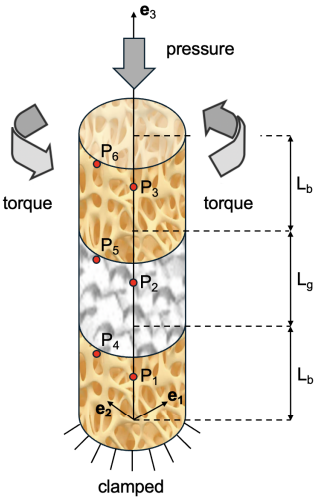

Figure 1. Schematic representation of the 3D system under study. The sample is constituted by two bone (B) regions and a graft (G) region in the middle in a BGB sequence. The sample is fully clamped at the bottom, while sinusoidal torque and pressure are applied to the top surface.

energy density and fluid–solid interactions over time. In other words, under our assumption, frequency load pertains exclusively to the slow time scale and thus can be interpreted as the cyclical process of loading and unloading over an extended period. Within the context of the well-separated time scale assumption, the frequency at the fast time scale is not considered, as it only indirectly influences the system through its effect on the effective amplitude of the mechanical load (see for more details [31]). The model parameters are reported in Table 1.

The numerical simulations have been performed through a finite element analysis using COMSOL Multiphysics.

4. Results and discussion

To analyze our numerical results, we consider six points inside the cylindrical specimen. Three of them (P_1, P_2, P_3) are located along the vertical axis of the cylinder at a height of 2.5, 7.5 and 12.5 cm. The points P_4, P_5, and P_6 are moved by 1.5 cm along the $\mathbf{e}_2$ axis to have probe points near the lateral surface of the sample (Figure 1).

In the first series of simulations, we have evaluated the impact of the frequency Ω on the system when $F_0 = 200$ MPa/m, $F_1 = 0.16$ MPa and $F_2 = 0.016$ MPa. These force amplitudes are numerically calibrated to produce a level of stimulus that stimulates the generation of new bone tissue. In essence, we consider the scenario where the stimulus S exceeds S_s, the synthesis threshold. Specifically, the maximum torque applied has an amplitude of 50.26 Nm, which is compatible with a reference value taken from the literature (see, e.g., [64]).

The first set of graphs in Figure 2 presents the evolution of the stimulus S over time at three different frequencies, specifically $\Omega = 0.01$ Cycles per unit Time (CpT) (Figure 2a,d), $\Omega = 0.1$ CpT (Figure 2b,e) and $\Omega = 1$ CpT (Figure 2c,f). At low frequency (i.e., $\Omega = 0.01$ CpT, Figure 2a,c), the stimulus response across all points is relatively flat, showing minimal growth, particularly at points P_1, P_3 and P_4, P_6, represented by the red lines. These points experience very low stimuli, suggesting either less mechanical interaction or areas of low strain, potentially in regions further from the loading centre or areas with less bone density. At intermediate frequency

Table 1. Structural parameters of the model used in the numerical simulations

L (cm)	15
r (cm)	2
L_b (cm)	5
L_g (cm)	5
$\hat{\rho}_b$ (kg/m^3)	1800
$\hat{\rho}_g$ (kg/m^3)	1800
ν	0.3
Y_b^{max} (GPa)	18
Y_g^{max} (GPa)	14.4
ν^v (N·s/m^2)	1×10^{-4}
k^v (N·s/m^2)	1×10^{-4}
s_b (s/m^2)	4.9×10^{-9}
r_b (s/m^2)	6.13×10^{-9}
r_g (s/m^2)	6.13×10^{-9}
κ (m^2/s)	1.6×10^{-4}
β	0.1
Ω (CpT)	0.01, 0.1, 1
F_0 (MPa/m)	200
F_1 (MPa)	0.16

(i.e. $\Omega = 0.1$ CpT, Figure 2b,e), the stimulus increases more significantly, with a sharp rise over time at certain points (notably P_1, P_4 and P_3, P_5, marked by blue and red lines, respectively). This response suggests that intermediate frequencies may optimize the mechanical environment to trigger a more substantial biological response. The green lines referring to the points in the graft (points P_2 and P_5) also show mild growth, indicating that these points are moderately responsive to frequency changes, though less active than the blue lines. This is because the stimulus originates from the osteocytes in bone tissue and then also reaches the graft with a slight delay. Finally, high-frequency loading (i.e., $\Omega = 1$ CpT, Figure 2c,f) leads to a much sharper increase in stimulus at points P_1, P_3 and P_4, P_6 (blue and red lines), suggesting that under these conditions, those points respond more significantly to mechanical stimulus. This could reflect a shift in the mechanical load distribution at higher frequencies, where, even initially, the less active points become more stimulated.

Figure 3 explores the evolution of the normalized bone mass density ρ_b^* over time, representing the gradual adaptation of bone tissue in response to the mechanical stimuli seen in Figure 2. The same points are analyzed under the three frequency regimes. Figure 3 panels (a) and (d) demonstrate a minimal change in bone mass density, with the points P_1, P_3 and P_4, P_6 (blue and red lines, respectively) maintaining the initial density value (i.e., $\rho_b^* = 0.5$), while bone density at the points P_2 and P_5 in the graft remains nearly equal to zero. This indicates that, at low frequencies, remodelling is minimal and bone mass density remains relatively static. At $\Omega = 0.1$ CpT (Figure 3b,e), bone mass density increases markedly over time for points P_1, P_3 and P_4, P_6 (blue and red lines, respectively). The points P_2 and P_5 (green lines) show little or no change, suggesting that these regions might experience less strain or be further from the main loading sites. Similarly to intermediate frequencies, Figure 3c and f show a pronounced increase in bone density for points P_1, P_3 and P_4, P_6 (blue and red lines, respectively) at $\Omega = 1$ CpT. This behaviour implies that high-frequency loading could significantly enhance the remodelling process, resulting in higher bone mass density. The nearly flat green lines (points P_2 and P_5) suggest that the regions associated with these points are less responsive even under high-loading conditions. Since this

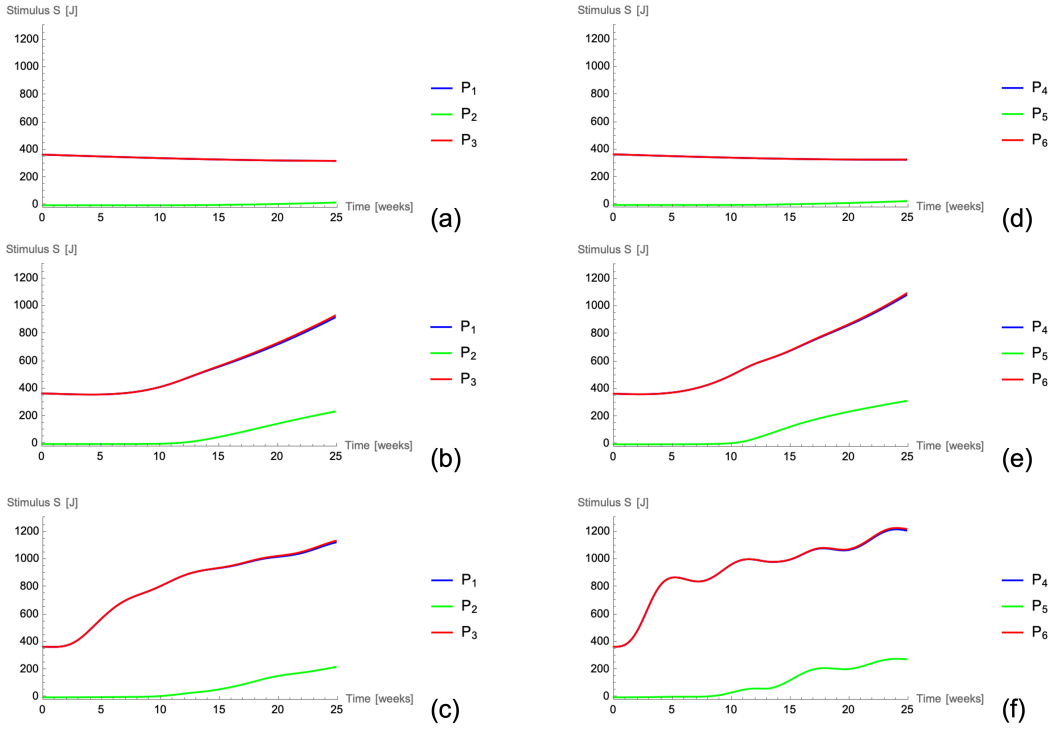

Figure 2. Influence of the frequency Ω on the stimulus S for points P_1, P_2, P_3 (a,b,c) and points P_4, P_5, P_6 (d,e,f). (a,d) $\Omega = 0.01$, (b,e) $\Omega = 0.1$ CpT, (c,f) $\Omega = 1$ CpT when $F_0 = 200$ MPa/m and $F_1 = 0.16$ MPa.

region is associated with the graft, this means that the production of the stimulus that is relevant in bone tissue is not yet sufficient to colonize the implant region and therefore has a relevant effect. Such results can also be observed in Figure 4a,b and c, where we show the distribution of the normalized bone mass density ρ_b^* in the 3D BGB structure at $t = 25$ weeks. One can observe that even with relatively low forces, increasing the frequency significantly enhances bone formation. This indicates that the cyclic nature of stimulation plays a crucial role in triggering remodelling responses in bone tissue.

Figure 5 focuses on the evolution of the normalized density of the graft mass ρ_g^* at the same points at different frequencies. Unlike bone mass density, the density of the graft mass appears to decrease across all points regardless of frequency. For low, intermediate and high frequencies, Figure 5 panels from (a) to (f) show a sharp decline in the density of the graft mass within the first few weeks. The green lines (points P_2 and P_5) fall to near zero after approximately 10–15 weeks. This behaviour suggests a process where the graft resorbs over time, potentially being replaced by newly formed bone tissue in a process characteristic of osteointegration, as it can be observed at intermediate and high frequency (Figure 3b,c,e,f). This type of study is crucial for assessing the timing of resorption and subsequent bone formation. In fact, if the graft is completely resorbed prior to bone tissue formation, the mechanical integrity of the system could be severely compromised.

To enhance osteointegration, we have increased the mechanical loads. While we observed that the pressure does not play any role even at higher values, torsion seems to affect the overall response of the BGB structure. Here, we report the results of a second series of simulations where $F_0 = 1000$ MPa/m, $F_1 = 0.16$ MPa and $\Omega = 0.1$ CpT.

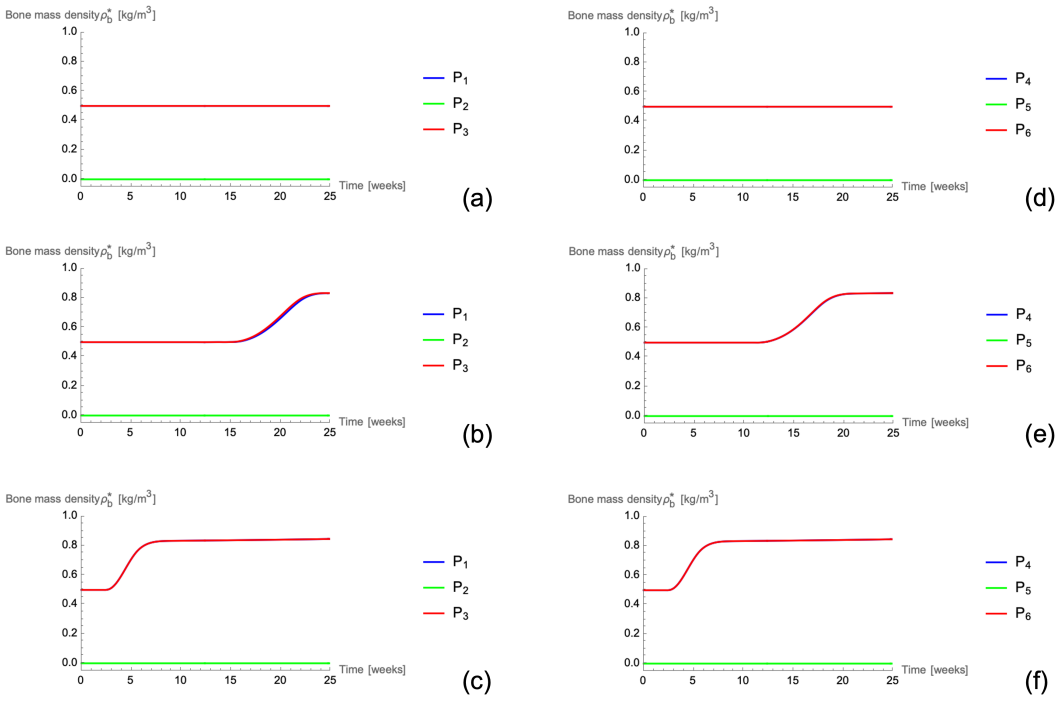

Figure 3. Influence of the frequency Ω on the normalized bone mass density ρ_b^* for points P_1, P_2, P_3 (a,b,c) and points P_4, P_5, P_6 (d,e,f). (a,d) $\Omega = 0.01$, (b,e) $\Omega = 0.1$ CpT, (c,f) $\Omega = 1$ CpT when $F_0 = 200$ MPa/m and $F_1 = 0.16$ MPa.

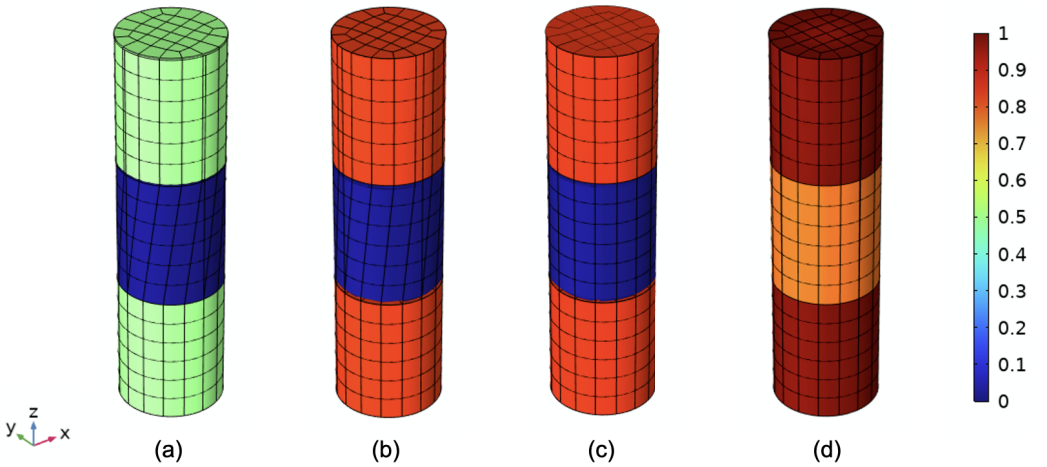

Figure 4. Normalized bone density ρ_b^2 at $t = 25$ weeks for $F_0 = 200$ MPa/m, $F_1 = 0.16$ MPa and $\Omega = 0.01$ CpT (a), $\Omega = 0.1$ CpT (b), $\Omega = 1$ CpT (c) and $F_0 = 1000$ MPa/m, $F_1 = 0.16$ MPa and $\Omega = 0.1$ CpT (d).

Figure 6 shows the temporal evolution of the stimulus S, the bone mass density ρ_b^*, and the graft mass density ρ_g^* for specific points P_1, P_2, P_3 (in plots a,b,c) and P_4, P_5, P_6 (in plots d,e,f). The curves in Figure 6a and d exhibit a smooth increase of the stimulus S for the points P_1, P_3

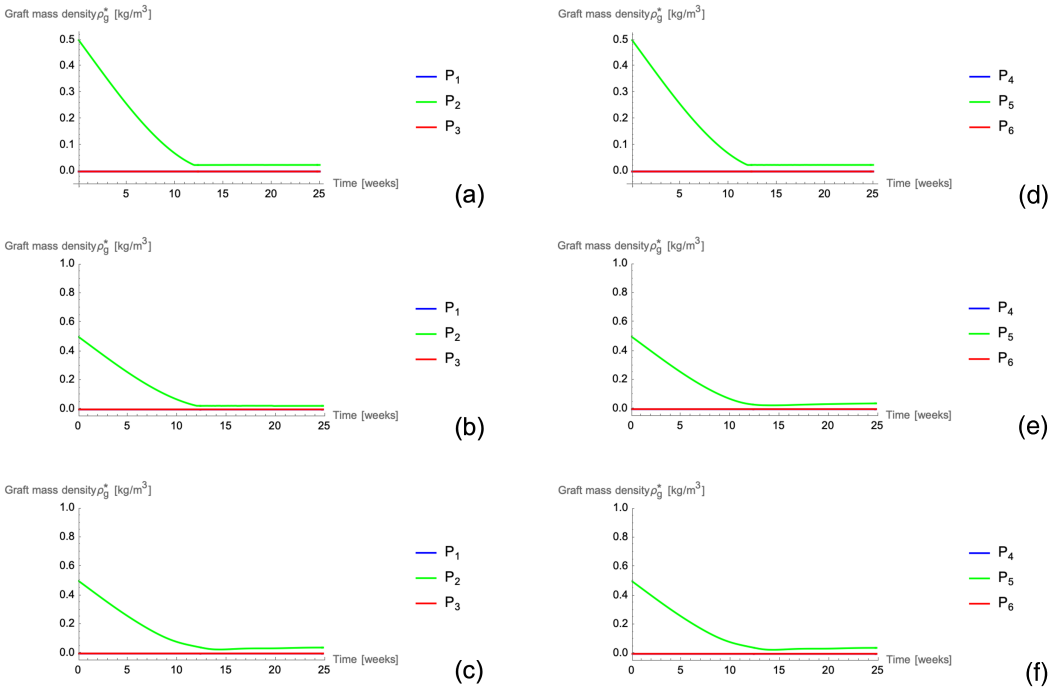

Figure 5. Influence of the frequency Ω on the graft normalized mass density ρ_g^* for points P_1, P_2, P_3 (a,b,c) and points P_4, P_5, P_6 (d,e,f). (a,d) $\Omega = 0.01$ CpT, (b,e) $\Omega = 0.1$ CpT, (c,f) $\Omega = 1$ CpT when $F_0 = 200$ MPa/m and $F_1 = 0.16$ MPa.

and P_4, P_6 (blue and red curves, respectively), while in the graft (points P_2 and P_5, green lines) S undergoes a steep upward trend after 10 weeks. Such values correlate with increased bone remodelling activity, which is consistent with what we see in bone density plots (Figure 6b,e). On the one hand, both in the bone and in the graft, ρ_b^* increases, reaching values of about 0.95 kg/m^3 and 0.85 kg/m^3 for points P_1, P_3, P_4, P_6 (blue and red lines) and P_2, P_5 (green lines), respectively. On the other hand, the density of the mass of the graft ρ_g^* is reduced at all points, meaning that the graft material is gradually resorbed or remodelled as bone tissue develops. Furthermore, depending on the level of the stimulus and its distribution over the sample, the mass density of the graft may remain different from zero before the generation of new bone tissue in the same region to prevent a possible rupture.

Overall, one can conclude that low-force and low-frequency loading result in minimal changes in bone density. At the same time, high-frequency and high-force conditions promote optimal bone growth and graft integration. Therefore, mechanical stimuli must be carefully calibrated in terms of both force and frequency to maximize bone growth and graft integration. For practical applications in bone grafts or orthopaedic implants, these results could guide the selection of rehabilitation protocols or the design of mechanical devices that apply controlled cyclic loading to encourage efficient bone regeneration and implant integration.

5. Conclusion

This study presents a 3D poromechanical model for simulating bone remodelling in systems incorporating bio-resorbable grafts, providing a detailed analysis of the interplay between mechanical loads and remodelling dynamics. Our results demonstrate that the application of dynamic

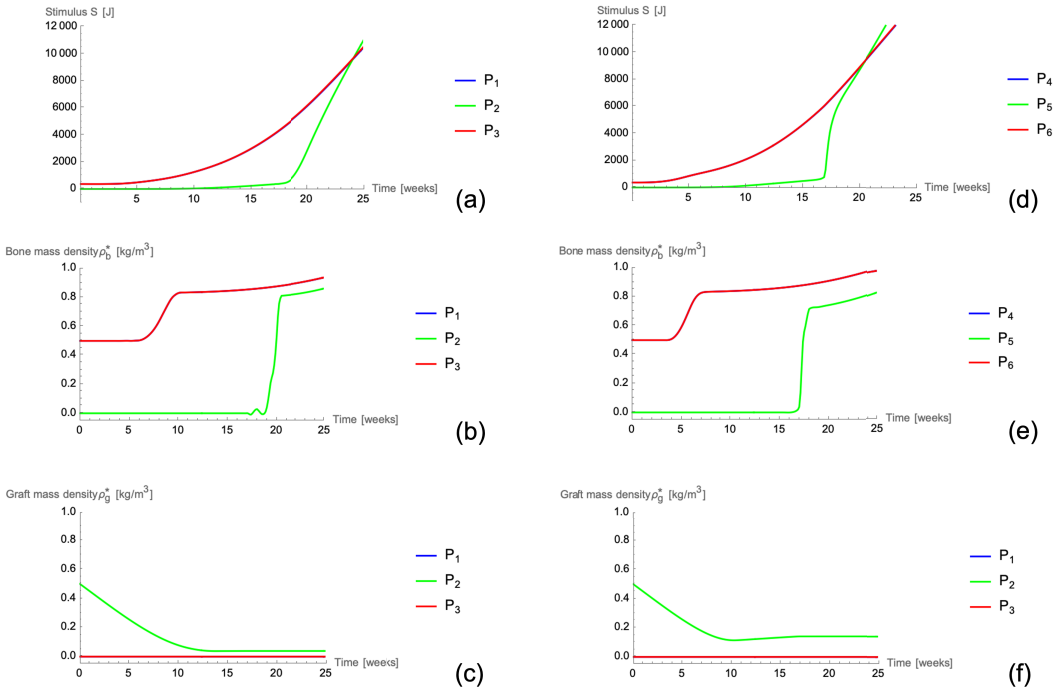

Figure 6. Evolution over time of the stimulus S, the bone normalized mass density ρ_b^* and the graft normalized mass density ρ_g^* for the points P_1, P_2, P_3 (a,b,c) and P_4, P_5, P_6 (d,e,f) when $F_0 = 1000$ MPa/m, $F_1 = 0.16$ MPa and $\Omega = 0.1$ CpT.

mechanical loads in a 3D BGB structure significantly influences both bone formation and graft resorption, emphasizing the importance of mechanical stimulation in scaffold integration. Unlike previous models that considered either dynamic loading in simplified geometries or studied 3D remodelling under static conditions, our approach combines these elements to capture the full spatial and temporal complexity of bone adaptation. The findings suggest that optimizing load frequency and intensity in a 3D environment can lead to improved bone regeneration, which has direct implications for the design of bioresorbable scaffolds and post-surgical rehabilitation strategies. More specifically, the simulations reveal that higher frequencies and load magnitudes enhance both bone regeneration and graft integration, while low mechanical loads yield poor remodelling effects from the clinical viewpoint.

The findings underscore the importance of calibrating mechanical loads in terms of intensity and frequency to optimize bone healing and scaffold integration. This model could serve as a valuable tool for improving the design of bio-resorbable grafts and developing targeted rehabilitation protocols. By capturing complex spatial and temporal interactions in bone/graft systems, the study could contribute to the advancement of both theoretical understanding and clinical applications in bone repair and regeneration. In future development, we want to add the effects of damage [65,66] and dissipation [67,68] to our model, since we believe that they play a crucial role in bone remodelling by driving biological processes that repair microdamage and maintain structural integrity, ensuring that the bone adapts effectively to mechanical stresses over time. This aspect will improve our understanding of the process and will allow us to add a crucial piece to the puzzle of bone remodelling.

Furthermore, bone remodelling is governed by cellular processes and external mechanical loads that occur over the course of minutes, while the comprehensive effects of this

mechanobiological phenomenon become evident after a duration of several weeks. The simultaneous presence of these two distinct time scales complicates the design of experiments aimed at evaluating and quantifying specific mechanical variables. Therefore, another objective of this paper is to present a modelling tool with sufficient accuracy for the planning of a measurement campaign, with the ultimate aim of validation. This methodological approach is crucial to ensure that experimental data are acquired in a manner that directly assesses model predictions while minimizing uncertainties and confounding factors. The use of a model as a guide can facilitate the validation process by identifying key predictions from the model, selecting measurable quantities, and optimizing experimental conditions. This involves determining the physical quantities predicted by the model (e.g., fluid pressure, strain fields, porosity effects on flow); identifying the most sensitive parameters, namely those that significantly influence the outcome and should be measured with high precision; selecting experimental variables that directly correspond to model outputs (e.g., pore pressure via pressure sensors, strain via digital image correlation or strain gauges, fluid flow via tracer experiments); considering the potential of indirect measurements (e.g., ultrasound or MRI for fluid flow) to provide the required data; utilizing the model to simulate various testing conditions to identify those that maximize the differentiation between hypotheses; ensuring that the selected conditions (e.g., loading frequency, amplitude, or boundary conditions) produce measurable responses; ensuring that experimental data are collected with adequate spatial and temporal resolution to capture significant model features; and minimizing measurement redundancy while ensuring ample data for robust validation.

Declaration of interests

The authors do not work for, advise, own shares in, or receive funds from any organization that could benefit from this article, and have declared no affiliations other than their research organizations.

Acknowledgments

The first author is supported by the Institut Universitaire de France.

References

[1] H. Frost, "A 2003 update of bone physiology and Wolffs Law for clinicians", *Angle Orthod.* **74** (2004), no. 1, pp. 3–15.

[2] C. Turner, "Three rules for bone adaptation to mechanical stimuli", *Bone* **23** (1998), no. 5, pp. 399–407.

[3] A. Robling, A. Castillo and C. Turner, "Biomechanical and molecular regulation of bone remodeling", *Annu. Rev. Biomed. Eng.* **8** (2006), pp. 455–498.

[4] L. Lanyon and C. Rubin, "Static vs dynamic loads as an influence on bone remodelling", *J. Biomech.* **17** (1985), no. 12, pp. 897–905.

[5] A. S. Morozova, E. N. Vilchevskaya, W. H. Müller and N. M. Bessonov, "Models for drug release of gentamicin in a polylactic acid matrix", *Math. Mech. Complex Syst.* **8** (2020), no. 4, pp. 307–320.

[6] S. Cowin, L. Moss-Salentijn and M. Moss, "Candidates for the mechanosensory system in bone", *J. Biomech. Eng.* **113** (1991), no. 2, pp. 191–197.

[7] R. Allena, D. Scerrato, A. Bersani and I. Giorgio, "A model for the bio-mechanical stimulus in bone remodelling as a diffusive signalling agent for bones reconstructed with bio-resorbable grafts", *Mech. Res. Commun.* **129** (2023), article no. 104094.

[8] M. Mullender and R. Huiskes, "Proposal for the regulatory mechanism of Wolff's law", *J. Orthopaed. Res.* **13** (1995), no. 4, pp. 503–512.

[9] R. Huiskes, R. Ruimerman, G. van Lenthe and J. Janssen, "Effects of mechanical forces on maintenance and adaptation of form in trabecular bone", *Nature* **405** (2000), no. 6787, pp. 704–706.

[10] I. Giorgio, F. dell'Isola, U. Andreaus, F. Alzahrani, T. Hayat and T. Lekszycki, "On mechanically driven biological stimulus for bone remodeling as a diffusive phenomenon", *Biomech. Model. Mechanobiol.* **18** (2019), no. 6, pp. 1639–1663.

[11] S. C. Cowin, "Bone poroelasticity", *J. Biomech.* **32** (1999), no. 3, pp. 217–238.

[12] R. Allena, D. Scerrato, A. Bersani and I. Giorgio, "Functional adaptation of bone mechanical properties using a diffusive stimulus originated by dynamic loads in bone remodelling", *Z. Angew. Math. Phys.* **75** (2024), article no. 85.

[13] P. Pivonka and C. Dunstan, "Role of mathematical modeling in bone fracture healing", *Bone Key Rep.* **1** (2012), pp. 221–230.

[14] D. Carter, D. Fyhrie and R. Whalen, "Trabecular bone density and loading history: regulation of connective tissue biology by mechanical energy", *J. Biomech.* **20** (1987), no. 8, pp. 785–794.

[15] T. Lekszycki and F. dell'Isola, "A mixture model with evolving mass densities for describing synthesis and resorption phenomena in bones reconstructed with bio-resorbable materials", *ZAMM - Z. Angew. Math. Mech.* **92** (2012), no. 6, pp. 426–444.

[16] A. Sheidaei, M. Kazempour, A. Hasanabadi, F. Nosouhi, M. Pithioux, M. Baniassadi, Y. Rémond and D. George, "Influence of bone microstructure distribution on developed mechanical energy for bone remodeling using a statistical reconstruction method", *Math. Mech. Solids* **24** (2019), no. 10, pp. 3027–3041.

[17] P. Germain, "The method of virtual power in the mechanics of continuous media, I: second-gradient theory", *Math. Mech. Complex Syst.* **8** (2020), no. 2, pp. 153–190.

[18] J. Chróścielewski, F. Dell'Isola, V. A. Eremeyev and A. Sabik, "On rotational instability within the nonlinear six-parameter shell theory", *Int. J. Solids Struct.* **196** (2020), pp. 179–189.

[19] V. A. Eremeyev, S. A. Lurie, Y. O. Solyaev and F. dell'Isola, "On the well posedness of static boundary value problem within the linear dilatational strain gradient elasticity", *Z. Angew. Math. Phys.* **71** (2020), pp. 1–16.

[20] L. Placidi, D. Timofeev, V. Maksimov, E. Barchiesi, A. Ciallella, A. Misra and F. dell'Isola, "Micro-mechano-morphology-informed continuum damage modeling with intrinsic 2nd gradient (pantographic) grain–grain interactions", *Int. J. Solids Struct.* **254** (2022), article no. 111880.

[21] F. dell'Isola, U. Andreaus and L. Placidi, "At the origins and in the vanguard of peridynamics, non-local and higher-gradient continuum mechanics: an underestimated and still topical contribution of Gabrio Piola", *Math. Mech. Solids* **20** (2015), no. 8, pp. 887–928.

[22] S. Federico, M. F. Alhasadi and A. Grillo, "Eshelby's inclusion theory in light of Noethers theorem", *Math. Mech. Complex Syst.* **7** (2019), no. 3, pp. 247–285.

[23] M. Tepedino, "The mechanical role of the periodontal ligament for developing mathematical models in orthodontics", *Math. Mech. Complex Syst.* **11** (2023), no. 4, pp. 525–539.

[24] A. Casalotti, F. D'Annibale and G. Rosi, "Optimization of an architected composite with tailored graded properties", *Z. Angew. Math. Phys.* **75** (2024), no. 4, article no. 126.

[25] E. Barchiesi, "Equilibria of axial-transversely loaded homogenized duoskelion beams", *Math. Mech. Complex Syst.* **12** (2024), no. 3, pp. 283–309.

[26] C. Soize, "An overview on uncertainty quantification and probabilistic learning on manifolds in multiscale mechanics of materials", *Math. Mech. Complex Syst.* **11** (2023), no. 1, pp. 87–174.

[27] G. La Valle, B. E. Abali, G. Falsone and C. Soize, "Sensitivity of a homogeneous and isotropic second-gradient continuum model for particle-based materials with respect to uncertainties", *ZAMM - Z. Angew. Math. Mech.* **103** (2023), no. 10, article no. e202300068.

[28] G. La Valle and C. Soize, "A higher-order nonlocal elasticity continuum model for deterministic and stochastic particle-based materials", *Z. Angew. Math. Phys.* **75** (2024), no. 2, article no. 49.

[29] C. Dissaux, L. Ruffenach, C. Bruant-Rodier, D. George, F. Bodin and Y. Rémond, "Cleft alveolar bone graft materials: literature review", *Cleft Palate-Craniofac. J.* **59** (2022), no. 3, pp. 336–346.

[30] V. Eremeyev, A. Skrzat and A. Vinakurava, "Application of the micropolar theory to the strength analysis of bioceramic materials for bone reconstruction", *Strength Mater.* **48** (2016), pp. 573–582.

[31] D. Scerrato, I. Giorgio, A. M. Bersani and D. Andreucci, "A proposal for a novel formulation based on the hyperbolic Cattaneo's equation to describe the mechano-transduction process occurring in bone remodeling", *Symmetry* **14** (2022), no. 11, article no. 2436.

[32] J.-F. Stoltz, J. Magdalou, D. George, Y. Chen, Y. Li, N. De Isla, X. He and Y. Remond, "Influence of mechanical forces on bone: introduction to mechanobiology and mechanical adaptation concept", *J. Cell. Immunother.* **4** (2018), no. 1, pp. 10–12.

[33] X. Zhang and A. Saraf, "Dynamic finite element modeling of bone adaptation to cyclic torsional loads", *J. Biomech.* **47** (2014), no. 10, pp. 2448–2454.

[34] D. Scerrato, A. M. Bersani and I. Giorgio, "Bio-inspired design of a porous resorbable scaffold for bone reconstruction: a preliminary study", *Biomimetics* **6** (2021), no. 1, article no. 18.

[35] F. dell'Isola, G. Sciarra and R. C. Batra, "Static deformations of a linear elastic porous body filled with an inviscid fluid", *J. Elast.* **72** (2003), pp. 99–120.
[36] F. dell'Isola and R. C. Batra, "Saint-Venant's problem for porous linear elastic materials", *J. Elast.* **47** (1997), pp. 73–81.
[37] F. dell'Isola, A. Madeo and P. Seppecher, "Boundary conditions at fluid-permeable interfaces in porous media: a variational approach", *Int. J. Solids Struct.* **46** (2009), no. 17, pp. 3150–3164.
[38] R. Burson and K. Enakoutsa, "Ductile void growing in micromorphic GLPD porous plastic solids containing two populations of cavities with different sizes", *Math. Mech. Complex Syst.* **10** (2023), no. 4, pp. 395–412.
[39] A. Madeo, F. dell'Isola and F. Darve, "A continuum model for deformable, second gradient porous media partially saturated with compressible fluids", *J. Mech. Phys. Solids* **61** (2013), no. 11, pp. 2196–2211.
[40] O. Coussy, *Poromechanics*, John Wiley & Sons: Chichester, 2004.
[41] E. F. Morgan, O. C. Yeh, W. C. Chang and T. M. Keaveny, "Nonlinear behavior of trabecular bone at small strains", *J. Biomech. Eng.* **123** (2001), no. 1, pp. 1–9.
[42] M. Biot, "General theory of three-dimensional consolidation", *J. Appl. Phys.* **12** (1941), no. 2, pp. 155–164.
[43] Y. Lu and T. Lekszycki, "Modelling of bone fracture healing: influence of gap size and angiogenesis into bioresorbable bone substitute", *Math. Mech. Solids* **22** (2017), no. 10, pp. 1997–2010.
[44] E. Bednarczyk and T. Lekszycki, "A novel mathematical model for growth of capillaries and nutrient supply with application to prediction of osteophyte onset", *ZAMP - Z. Angew. Math. Phys.* **67** (2016), no. 4, pp. 1–14.
[45] M. A. Biot, "Mechanics of deformation and acoustic propagation in porous media", *J. Appl. Phys.* **33** (1962), no. 4, pp. 1482–1498.
[46] S. C. Cowin and J. W. Nunziato, "Linear elastic materials with voids", *J. Elast.* **13** (1983), no. 2, pp. 125–147.
[47] M. Olive, "Effective computation of SO(3) and O(3) linear representation symmetry classes", *Math. Mech. Complex Syst.* **7** (2019), no. 3, pp. 203–237.
[48] N. Branecka, M. E. Yildizdag, A. Ciallella and I. Giorgio, "Bone remodeling process based on hydrostatic and deviatoric strain mechano-sensing", *Biomimetics* **7** (2022), no. 2, article no. 59.
[49] N. Branecka, M. Shanehsazzadeh, M. E. Yildizdag and I. Giorgio, "A bone remodeling model involving two mechanical stimuli originated from shear and normal load conditions within the 3D continuum mechanics framework", *Contin. Mech. Thermodyn.* **37** (2024), no. 1, article no. 7.
[50] I. Giorgio, F. dell'Isola, U. Andreaus and A. Misra, "An orthotropic continuum model with substructure evolution for describing bone remodeling: an interpretation of the primary mechanism behind Wolff's law", *Biomech. Model. Mechanobiol.* **22** (2023), no. 6, pp. 2135–2152.
[51] P. Heinemann and M. Kasperski, "Damping induced by walking and running", *Proc. Eng.* **199** (2017), pp. 2826–2831.
[52] E. F. Eriksen, "Cellular mechanisms of bone remodeling", *Rev. Endocr. Metab. Disord.* **11** (2010), no. 4, pp. 219–227.
[53] S. R. Eugster, "Numerical analysis of nonlinear wave propagation in a pantographic sheet", *Math. Mech. Complex Syst.* **9** (2022), no. 3, pp. 293–310.
[54] L. Placidi, F. Di Girolamo and R. Fedele, "Variational study of a Maxwell–Rayleigh-type finite length model for the preliminary design of a tensegrity chain with a tunable band gap", *Mech. Res. Commun.* **136** (2024), article no. 104255.
[55] A. Grillo and S. Di Stefano, "Comparison between different viewpoints on bulk growth mechanics", *Math. Mech. Complex Syst.* **11** (2023), no. 2, pp. 287–311.
[56] A. Grillo and S. Di Stefano, "An a posteriori approach to the mechanics of volumetric growth", *Math. Mech. Complex Syst.* **11** (2023), no. 1, pp. 57–86.
[57] M. Valmalle, B. Smaniotto, M. Spagnuolo, A. Ciallella and F. Hild, "Mesoscale DVC analyses and parameter calibration for pantographic block in 3-point flexure", *Eur. J. Mech.-A/Solids* **101** (2023), article no. 105063.
[58] G. Aydin, M. E. Yildizdag and B. E. Abali, "Strain-gradient modeling and computation of 3-d printed metamaterials for verifying constitutive parameters determined by asymptotic homogenization", in *Theoretical Analyses, Computations, and Experiments of Multiscale Materials: A Tribute to Francesco dell'Isola*, Springer: Cham, 2022, pp. 343–357.
[59] H. Yang, B. E. Abali, W. H. Müller, S. Barboura and J. Li, "Verification of asymptotic homogenization method developed for periodic architected materials in strain gradient continuum", *Int. J. Solids Struct.* **238** (2022), article no. 111386.
[60] R. Fedele, L. Placidi and F. Fabbrocino, "A review of inverse problems for generalized elastic media: formulations, experiments, synthesis", *Contin. Mech. Thermodyn.* **36** (2024), no. 6, pp. 1413–1453.
[61] A. Misra, L. Placidi, F. dell'Isola and E. Barchiesi, "Identification of a geometrically nonlinear micromorphic continuum via granular micromechanics", *Z. Angew. Math. Phys.* **72** (2021), pp. 1–21.
[62] L. Greco, A. Scrofani and M. Cuomo, "A non-linear symmetric G1-conforming Bézier finite element formulation for the analysis of Kirchhoff beam assemblies", *Comput. Methods Appl. Mech. Eng.* **387** (2021), article no. 114176.

[63] L. V. Tran and J. Niiranen, "A geometrically nonlinear Euler–Bernoulli beam model within strain gradient elasticity with isogeometric analysis and lattice structure applications", *Math. Mech. Complex Syst.* **8** (2020), no. 4, pp. 345–371.

[64] G. M. Kotzar, D. T. Davy, J. Berilla and V. M. Goldberg, "Torsional loads in the early postoperative period following total hip replacement", *J. Orthopaed. Res.* **13** (1995), no. 6, pp. 945–955.

[65] L. Placidi, E. Barchiesi, F. Dell'Isola, V. Maksimov, A. Misra, N. Rezaei, A. Scrofani and D. Timofeev, "On a hemi-variational formulation for a 2D elasto-plastic-damage strain gradient solid with granular microstructure", *Math. Eng.* **5** (2022), pp. 1–24.

[66] J. M. T. Espino, J. H. E. Sandoval, C. A. Tran, et al., "Validation of a hemi-variational block-based approach to the modelling of common in-plane failures in masonry structures", in *Sixty Shades of Generalized Continua: Dedicated to the 60th Birthday of Prof. Victor A. Eremeyev*, Springer: Cham, 2023, pp. 191–210.

[67] O. Chekeres, V. Salnikov and F. D'Annibale, "From approximation of dissipative systems to representative space-time volume elements for metamaterials", *Contin. Mech. Thermodyn.* **36** (2024), no. 6, pp. 1597–1605.

[68] M. Cuomo, L. Contrafatto and L. Greco, "A cohesive interface model with degrading friction coefficient", *Math. Mech. Complex Syst.* **12** (2024), no. 2, pp. 113–133.